WAKE GEOMETRY CALCULATIONS FOR TILT-ROTOR USING VISCOUS VORTEX METHOD

Wei Peng(魏鹏), *Shi Yongjie*(史勇杰), *Xu Guohua*(徐国华)

(Science and Technology on Rotorcraft Aeromechanics Laboratory, Nanjing University of Aeronautics and Astronautics, Nanjing, 210016, P. R. China)

Abstract: A tilt-rotor unsteady flow analytical method has been developed based upon viscous vortex-particle method. In this method, the vorticity field is divided into small assembled vortex particles. Vortex motion and diffusion are obtained by solving the velocity-vorticity-formed incompressible Navier-Stokes equations using a grid-free Lagrangian simulation method. Generation of the newly vortex particles is calculated by using the Weissinger-L lifting surface model. Furthermore, in order to significantly improve computational efficiency, a fast multiple method (FMM) is introduced into the calculation of induced velocity and its gradient. Finally, the joint vertical experimental (JVX) tilt-rotor is taken as numerical examples to analyze. The wake geometry and downwash are investigated for both hover and airplane modes. The proposed method for tilt-rotor flow analysis is verified by comparing its results with those available measured data. Comparison indicates that the current method can accurately capture the complicated tilt-rotor wake variation and be suitable for aerodynamic interaction simulation in complex environments. Additionally, the aerodynamic interactional characteristics of dual-rotor wake are discussed in different rotor distance. Results show that there are significant differences on interactional characteristics between hover mode and airplane mode.

Key words: tilt-rotor; rotor wake; viscous vortex method; aerodynamic interaction

CLC number: V211.52 **Document code**: A **Article ID**: 1005-1120(2013)04-0297-09

INTRODUCTION

Tiltrotor aircrafts such as XV-15 and V-22 are unique because they combine the vertical take-off and landing capability of the helicopter with the high-speed cruise performance of fixed-wing turboprop aircraft. It is anticipated that, tilt-rotor aircraft will play a more important role in both the military and civilian aviation transportation in the future.

When a tilt-rotor operates in helicopter mode, such as hover and vertical taking off, its rotor wake remains in the vicinity of the blades and induces a highly non-linear velocity field, which has a strong impact on the rotor and wing aerodynamic performance, aerodynamic noise and dynamics etc. So far, rotor wake prediction has still one of the most challenging issues for tiltrotor aerodynamics because of the complexity of the wake dynamics.

Previous work on tilt-rotor wake prediction was limited, in part by the absence of appropriate measured data. Recently, computational fluid dynamics (CFD) technology finds application in computing wake and Refs. [1-5] contain a sampling of published results for CFD simulations. Although CFD method can directly capture the wake without additional wake models, the numerical dissipation inherent in this method tends to dampen high-intensity vortical structures. Furthermore, huge computation resource and time cost needed in solution also become barriers for

Foundation item: Supported by the National Natural Science Foundation of China (11302103).

Received date: 2012-10-30; **revision received date**: 2013-01-19

Corresponding author: Shi Yongjie, Associate Professor, E-mail: shiyongjie@nuaa.edu.cn.

wake capturing computation. An alternative methodology is Lagrangian vortex method which can capture tip vortex well and be more efficient when compared with the Eulerian CFD method. Acree[6] used a multiple-trailer free-wake model to predict the hover performance as well as the airplane mode performance. The results indicate that the improved free-wake model is capable to predict tilt-rotor wake. However, the traditional free-wake method has to rely on empirical parameters, such as the vortex core model, rolled-up tip vortex model.

In 2009 and 2010, He and Zhao[7-8] developed a new viscous wake model based on vortex particle method (VPM) which is different from traditional non-viscous freewake model. Their results show that the VPM method can capture the fundamental characteristics of the helicopter rotor wake vorticity interaction, especially is ideal in capturing and maintaining the unsteady compact vortical structures that shed off the helicopter blades.

In present paper, different from He and Zhao′s work, the viscous vortex method is extended to predict tilt-rotor wake dynamics. And a new tilt-rotor unsteady flow analytical method is established. Compared with a helicopter blade, a tilt-rotor blade has thicker airfoils with larger built-in twist and operates at higher tip speeds with higher loading, which results in very different induced velocity distributions. To include three-dimensional effects of blade, the Weissinger-L (W-L) theory is also employed to solve the circulation of bound vortex and newly generated vortex particles in this paper. Furthermore, the fast multiple method (FMM) method is introduced to accelerate the calculation of induced velocity and its gradient which is very time-comsuming.

1 METHODOLOGY

For a simple demonstration, Fig. 1 gives the schematic of current model. As illustrated, the rotor wake variation is predicted using the viscous vortex method, and the vorticity of newly generated particles is solved by the W-L lifting surface model.

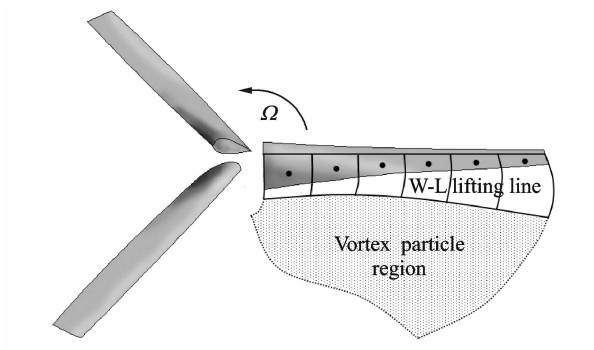

Fig. 1 Schematic of present model

1.1 Viscous vortex method

The airflow around rotorcraft is incompressible except for a very small region around the rotor blade tip. Therefore, rotor wake dynamic can be described by vorticity-velocity formulation of incompressible Navier-Stokes equation

$$\frac{\mathrm{d}\boldsymbol{\omega}}{\mathrm{d}t}=\boldsymbol{\omega}\cdot\nabla\boldsymbol{u}+\nu\nabla^2\boldsymbol{\omega} \tag{1}$$

where $\boldsymbol{\omega}=\nabla\times\boldsymbol{u}$ is the vorticity, $\boldsymbol{u}(x,t)$ the velocity, and ν the kinematic viscosity.

In the viscous vortex method, the rotor wake field is represented by a set of Lagrangian, vector-valued particles

$$\boldsymbol{\omega}_\varepsilon(\boldsymbol{x},t)=\sum_p\boldsymbol{\alpha}_p(t)\zeta_\varepsilon[\boldsymbol{x}-\boldsymbol{x}_p(t)] \tag{2}$$

where $\boldsymbol{x}_p(t)$ is the particle′s position and $\boldsymbol{\alpha}_p(t)$ vector strength. The smooth cutoff function $\zeta_\varepsilon(\boldsymbol{x})$ is defined by

$$\zeta_\varepsilon(\boldsymbol{x})=\frac{1}{\varepsilon^3}\zeta\left(\frac{|\boldsymbol{x}|}{\varepsilon}\right) \tag{3}$$

where ε is the smoothing parameter, and the Gaussian distribution is used in present method.

$$\zeta(\boldsymbol{x})=\frac{1}{(2\pi)^{3/2}}\mathrm{e}^{-x^2/2} \tag{4}$$

The vortex particle moves along with the local flow, and the position $\boldsymbol{x}_p$ is governed by the following equation

$$\frac{\mathrm{d}\boldsymbol{x}_p(t)}{\mathrm{d}t}=\boldsymbol{u}(\boldsymbol{x}_p,t) \tag{5}$$

where $\boldsymbol{u}(\boldsymbol{x}_p,t)=\boldsymbol{u}_\infty+\boldsymbol{u}_{p(\mathrm{ind})}$. For the Gaussian smoothing, the induced velocity $\boldsymbol{u}_{p(\mathrm{ind})}$ is obtained as[9]

$$\boldsymbol{u}_{p(\mathrm{ind})}=-\hat{\varepsilon}^{-3}\sum_{q=1}^{N}\frac{G(\rho)-\zeta(\rho)}{\rho^2}(\boldsymbol{x}_p-\boldsymbol{x}_q)\times\boldsymbol{\alpha}_q \tag{6}$$

where $\hat{\varepsilon}=\sqrt{\varepsilon_p^2+\varepsilon_q^2}/2$ is the symmetrized smoothing parameter, $\rho=|\boldsymbol{x}_p-\boldsymbol{x}_q|/\hat{\varepsilon}$ the non-dimensional distance. The Green function is defined as

$$G(\rho)=\frac{1}{4\pi\rho}Erf\left(\frac{\rho}{\sqrt{2}}\right) \tag{7}$$

For vortex methods, straight-forward evaluation of Eq. (6) requires $O(N^2)$ operations (evaluating self-induced velocity of N particles). It will make the method unacceptable for simulations when N is large. Therefore, a fast computational algorithm is needed to accelerate the calculation process, which will be described in later section.

At each time step, the circulation change due to 3D stretch is computed by

$$\left(\frac{\mathrm{d}\boldsymbol{\alpha}_p}{\mathrm{d}t}\right)_{\mathrm{ST}}=[\nabla\boldsymbol{u}(\boldsymbol{x}_p,t)]^{\mathrm{T}}[\boldsymbol{\alpha}_p] \tag{8}$$

This formulation offers the advantage of conserving the total circulation[9]. It should be noted that the calculation of the velocity gradient with direct summation also requires $O(N^2)$ computation cost. Therefore, the fast method is also needed in evaluating the velocity gradient.

The circulation change due to viscous diffusion is solved by using the technique of particle strength exchange (PSE)[9-10]. In the PSE algorithm the evolution equation for the particle circulation becomes

$$\left(\frac{\mathrm{d}\boldsymbol{\alpha}_p}{\mathrm{d}t}\right)_{\mathrm{VDT}}=\nu\nabla^2\boldsymbol{\alpha}_p=\frac{2\nu}{\hat{\varepsilon}^2}\sum_q(V_p\boldsymbol{\alpha}_q-V_q\boldsymbol{\alpha}_p)\eta_{\hat{\varepsilon}}(\boldsymbol{x}_p-\boldsymbol{x}_q) \tag{9}$$

where V is the volume of the vortex particles, and $\eta_\varepsilon=\varepsilon^{-3}\eta(\boldsymbol{x}/\varepsilon)$ the cutoff function. For the Gaussian smoothing, $\eta_\varepsilon=\zeta_\varepsilon$.

1.2 Generation of new vortex particles

In present model, the blade surface is treated as the only vorticity source that generates vortex particles into the rotor wake, and the circulation of the blade bound vortex and new vortex particles are calculated by using the W-L lifting surface model which can include blade three-dimensional effects.

A schematic of the W-L model is shown in Fig. 2, where the blade is divided into N_s spanwise panels with the bound circulation located along the quarter-chord line. A control point on each panel is placed at the 3/4-chord location. The trailed wake vortices extend downstream from the blade bound vortex segment end points, located along the quarter-chord. By applying no-penetration boundary condition, the blade bound circulation can be represented as

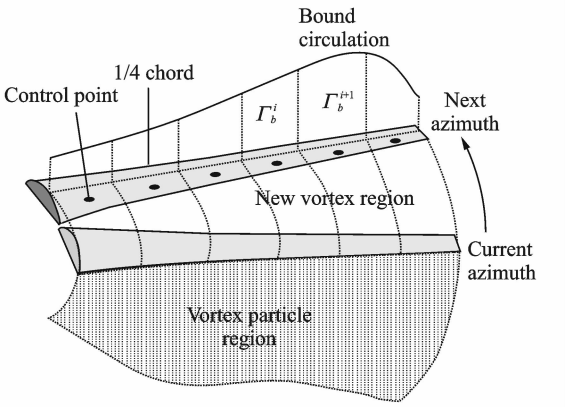

Fig. 2 Schematic of new vortex particle generation based on W-L model

$$\begin{bmatrix}a_{11}&\cdots&a_{1N}\\ \vdots&\ddots&\vdots\\ a_{N1}&\cdots&a_{NN}\end{bmatrix}\begin{bmatrix}\Gamma_{b1}\\ \vdots\\ \Gamma_{bN}\end{bmatrix}=\begin{bmatrix}b_1\\ \vdots\\ b_N\end{bmatrix} \tag{10}$$

or $\boldsymbol{A}\boldsymbol{\Gamma}_b=\boldsymbol{B}$.

The vorticity flux process is carried out in respect of Kelvin's circulation theorem, which provides a constraint on the total circulation strength. At each time step, the vorticity source created at each blade segment and shed into the rotor wake can be written as[7]

$$\gamma_\omega=-\frac{\mathrm{d}\Gamma_b}{\mathrm{d}t}+\boldsymbol{v}_b\nabla\cdot\Gamma_b \tag{11}$$

1.3 Fast multiple method (FMM)

As previously mentioned, the evaluation of the particle convection velocity and velocity gradient is time consumed and requires the fast algorithm to reduce the computation cost. There are two major categories of fast summation methods discussed in the literature. One is the TreeCode method[11] and the other is FMM[12]. In general, FMM is more efficient compared with TreeCode method as the former requires only $O(N)$ operations. In this study, the FMM algorithm is implemented.

In the FMM algorithm, the computational domain is divided into tree data structure (as shown in Fig. 3). For the adjacent particles, the influence must be calculated directly (P2P). If they are far away from each other, the influence of the source particle cluster on the target particle cluster is obtained in the following steps: (1) Computing multiple expansion from particles (P2M), (2) translating the multiple expansion to local expansion (M2L), (3) computing velocity and velocity gradient by using the local expansion (L2P).

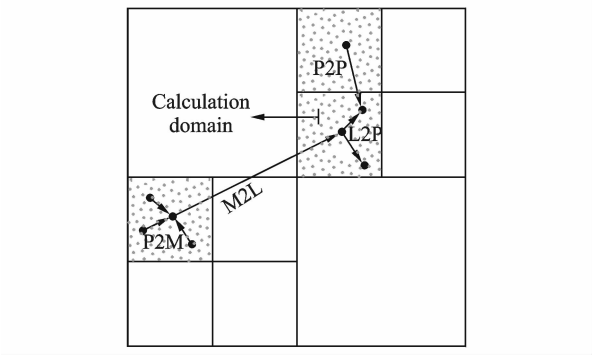

Fig. 3 Illustration of two-dimensional FMM algorithm

To further improve computational efficiency, an adaptive oct-tree method is used to divide the computation region (see Fig. 4). Based on multi-level data structure, the far-field interaction between vortex elements is computed by a layer by layer operation.

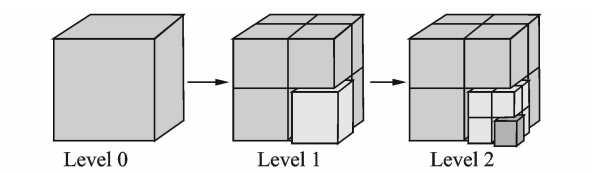

Fig. 4 Schematic of domain partition by using Oct-tree

As a brief summary of the above methods, Fig. 5 presents the flow chart of the current method.

2 RESULTS AND DISCUSSION

In this section, the viscous vortex method is used to investigate the rotor wake dynamics and the wake interactional characteristics of dual-rotors in the helicopter and airplane modes. For all the simulations next, the joint vertical experimental (JVX) rotor[6,13] is used. JVX is a 0.658-scale model of an early V-22 tilt-rotor configuration with higher solidity obtained by increasing the chord by 8.4% along the span. The isolated rotor was tested in the NASA Ames Research Center Outdoor Aerodynamic Research Facility (OARF) in 1984[13]. The main physical characteristics of the rotor are presented in Table 1, and the twist distribution is shown in Fig. 6, where r/R represents the blade radius.

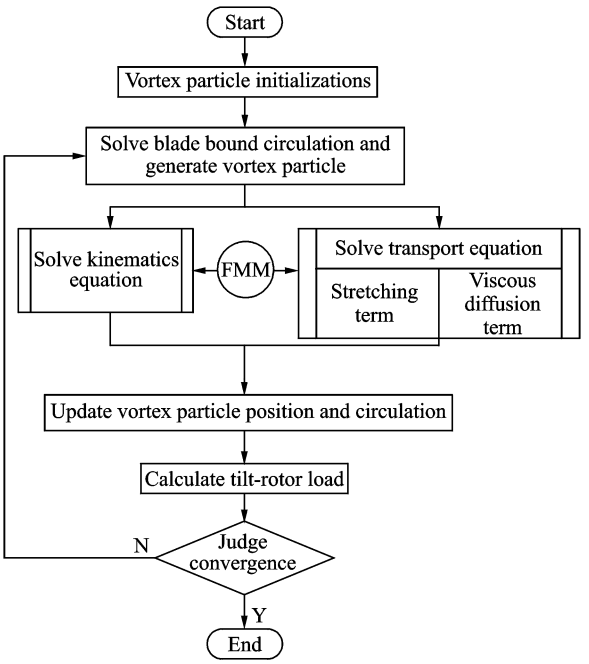

Fig. 5 Flow chart of rotor flow field calculation model based on viscous vortex model

Table 1 Parameters of JVX rotor

Radius/m	Solidity	Tip chord/m	Taper
3.81	0.113 8	0.401	0.65

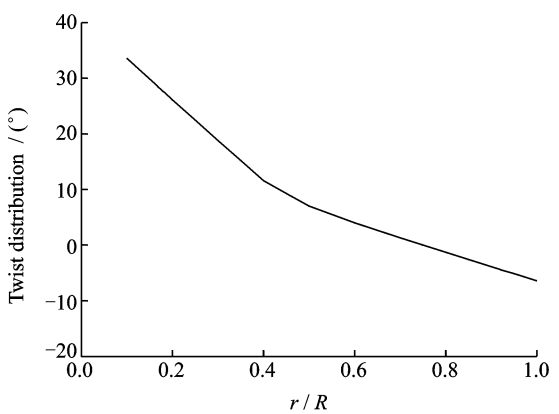

Fig. 6 Twist distribution of rotor blade

2.1 Single-rotor cases

To validate the developed model for rotor flow field analysis, several cases for single-rotor are tested and compared with the available measured data[13].

Fig. 7 shows the predicted time-averaged downwash at vertical position $z=0.4R$ in hover. For comparison, the figure also gives the calculated results of the free-wake. As shown in Fig. 7, the vortex particle predictions agree well with the measured data at both pitch conditions and they are more accurate compared with free-wake results. The measured downwash profile also shows that the downwash decreases rapidly around $r/R=0.8$ which indicates the rotor wake quickly contracts after leaving the rotor plane. Additionally, the wake contraction radius varied with collective pitch is also shown in Fig. 7, and it is observed that the contraction of the rotor wake is more serious at small collective-pitch condition.

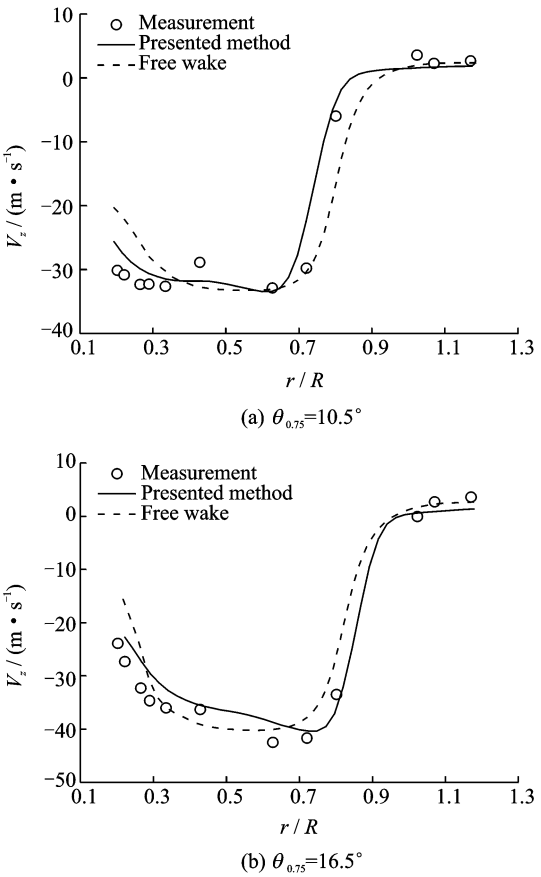

Fig. 7 Radial distribution of rotor induced downwash

For further insight into the phenomenon of varied wake contraction along with the collective pitch, Fig. 8 gives the spanwise bound circulation distribution at different collective pitches. It is seen that bound circulation changes insensiblly over the working portion of the blade (about $0.3R$—$0.8R$) at the condition of large collective pitch. But near the tip, circulation decreases rapidly and results in a strong tip vortex. In contrast, at small collective-pitch, circulation decreases over working portion and the vorticity distribution of shear layer is very different from large collective-pitch condition, which agrees well with the results in Ref. [6]. Under this condition, a strong vortex will be rolled-up at the position toward inboard rather than the blade tip region. For these reasons, the conventional rolled-up tip vortex model used in free wake methodology is invalid for highly twisted blades at low thrust. Comparatively, current model does not have this problem and is more suitable for tilt-rotor application.

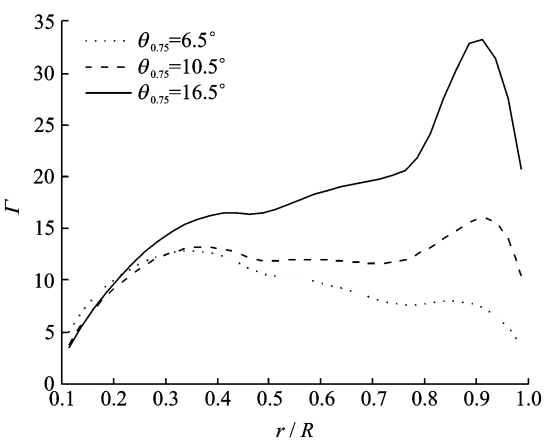

Fig. 8 Predicted radial distribution of bound circulation

Above conclusions indicate that, the induced velocity distributes more smoothly in tilt-rotor hover-flowfield because of the highly twisted characteristics of blade. And the rotor bound circulation distribution also differ with that of traditional helicopter. In order to further analyze the influence of blade highly twisted characteristics on tiltrotor wake, a reference rotor with untwisted blade is comparatively analyzed here. This

reference rotor has the same parameters as JVX model except for blade twist.

Fig. 9 presents the vortex particle distribution for the above two rotors at different collective pitch conditions. In Fig. 9, small spheres are used on behalf of the vortex particles, and the volume of a sphere represents the vortex particle circulation. As seen in Fig. 9, the tip vortex characteristics of JVX rotor are not so obvious compared with the reference rotor with untwisted blade. Especially for the collective pitch $\theta_{0.75} = 6.5°$, vortex particles distributed in the blade tip region are not so concentrated as two other conditions.

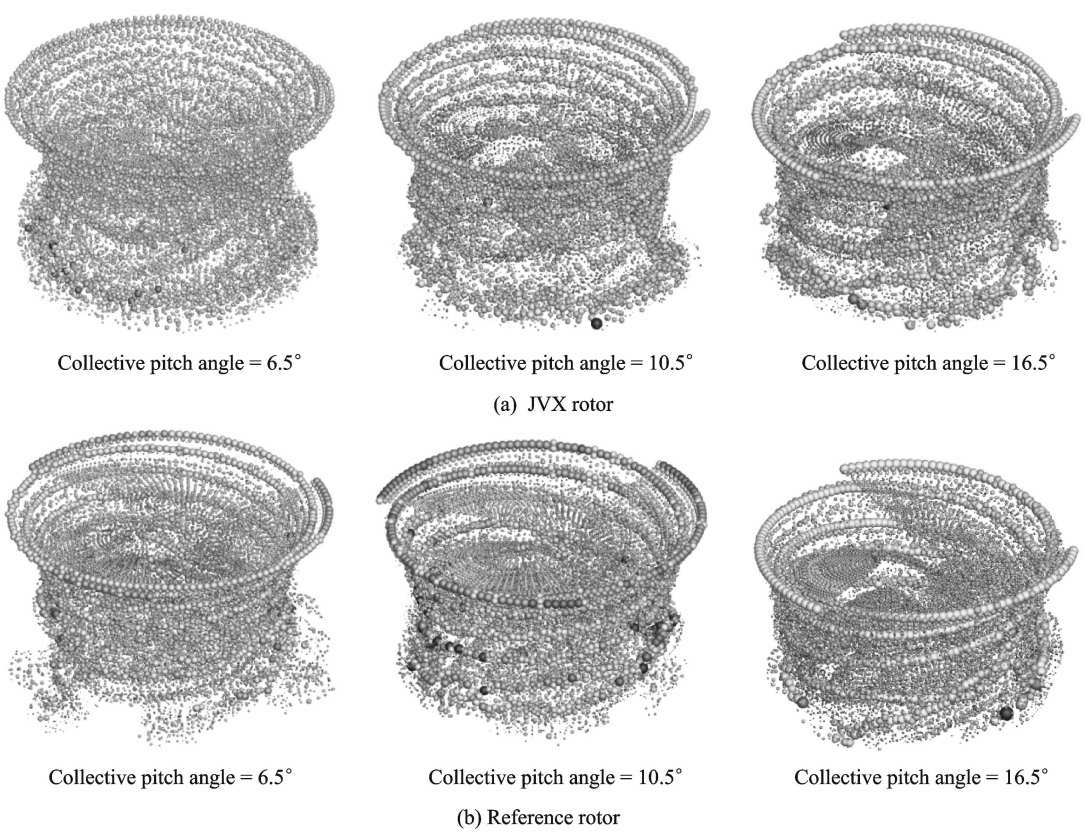

Fig. 9 Vortex particle transient distribution

Tip vortex displacements for the above two rotors with two different collective pitches are comparetively shown in Fig. 10. It is found that, tip vortex axial displacements of the reference rotor are bigger than that of the JVX rotor for both collective pitch conditions. And this characteristic is more obvious especially at the small collective pitch condition. Tip vortex radial displacements present similar phenomenons to tip vortex axial displacements but are not so obvious. The main reason of the above phenomenon can be analyzed through the wake characteristic shown in Fig. 8. The radial displacement of tip vortex is mostly affected by its self-interaction, whereas the axial displacement mainly relates to whole induced inflow. The tip vortex of reference rotor with untwisted blades is more strong compared with the JVX rotor. Therefore, the tip vortex self-interaction of the reference rotor is more obvious than that of the JVX rotor, and leads to faster contraction after the tip vortex leaves the blade. At the same time, the untwisted design of reference rotor will also cause the induced inflow different from the JVX rotor even for the same collective pitch, and this difference will directly result in the different axial displacement of tip vortex.

2.2 Interactional wake of dual-rotor

The side-by-side rotor configuration of tilt-

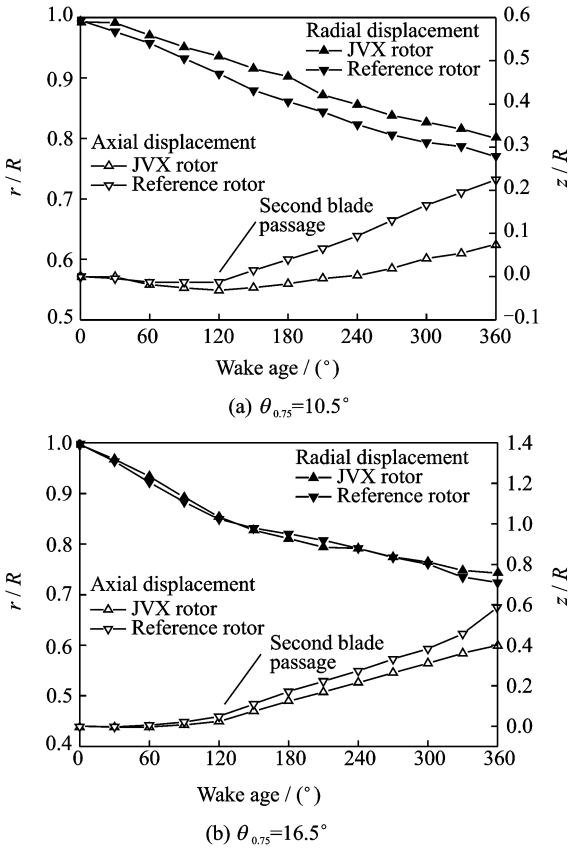

Fig. 10 Comparison of tip vortex axial and radial displacements

rotor aircraft leads to strong mutual interactions between the dual-rotors, and then it will cause a serious impact on the aerodynamic performance. In this section, several test cases are performed to investigate the interactional effect of the wake in dual-rotor configuration in helicopter and airplane-mode. In these test cases, the distance between the dual-rotor hub center is set to $L=2.4R$ and $L=3.0R$.

Fig. 11 shows the transient distribution of vortex particles at $L=2.4R$ condition. It can be seen that, compared with the single rotor wake, dual-rotor wake presents serious interference phenomenon. And due to the common induced effect of both sides of the rotor, the flow field appears upward flow in the region between the two rotors. This forms the unique fountain effects of tilt-rotor flowfeild. Influenced by this upwash, part of the wake shows the trend of upward movement. This will lead to the appearance of instability vortex area near the rotor disk, thus affecting the rotor aerodynamic characteristics. It is worth noting, in the actual situation, due to the blocking effect of the wing, the tilt-rotor fountain flow field will be more obvious than that without wing. But what can be drawn from above is that, the dual-rotor interference plays a key role in the formation of the tilt-rotor fountain flow field. In other words, the single rotor flow field does not form fountain effect in any case.

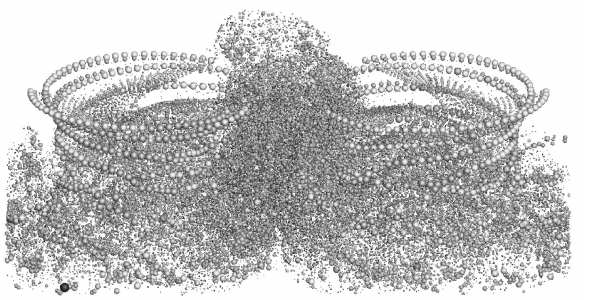

Fig. 11 Vortex particle transient distribution of dual-rotor ($L=2.4R$)

Fig. 12 presents the vorticity contour over a vertical plane passing through the rotor hub center for $L=2.4R$. Similar to helicopter rotor wake, the predicted tilt-rotor wake also quickly contracts immediately below the rotor plane. The difference is the strong interference appeared in the side close to each other. Due to the strong interaction, rotor tip vortex breaks down soon when convected further downstream. Because the interaction region is near the rotor disk, the unstable state of wake will influence the rotor aerodynamic characteristics. Especially in the descending flight process, unbalance of lift between left and right rotors will easily lead the single rotor into vortex ring state, which will be a potential safety hazard to the tilt-rotor aircraft. On the April 8, 2000, when a flight of MV-22 of U. S. Marines was conducting a night assault mission, it just got into the vortex ring state because of the rapidly descent speed and eventually crashed.

To gain further insight into the wake interaction, Fig. 13 shows the predicted time averaged

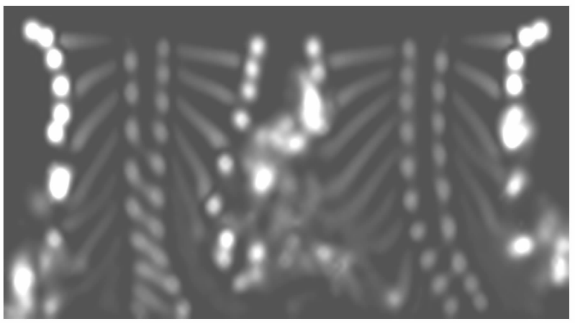

Fig. 12 Vorticity contour over a cross section through rotor hub center

downwash of left rotor along the rotor lateral axes at different planes. In this figure, the induced velocity exhibits an asymmetric pattern due to the interaction from wake of another rotor. The downwash is much smaller in the side close to each other and this phenomena is more obvious with small distacne.

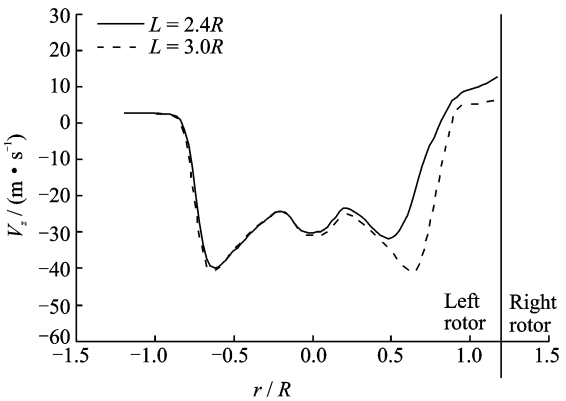

Fig. 13 Radial distribution of induced downwash under left rotor in hover

Finally, the airplane-mode performance is investigated. Fig. 14(a) presents the simulated rotor wake vorticity iso-surfaces. It is shown that the rotor wake will be blown away from the rotor plane quickly due to the large flight speed in this mode. Therefore the rotor wake is not obviously interfered and distorted, and the wake interaction becomes much weaker. Fig. 14(b) presents the time averaged downwash behind the left rotor in airplane mode. Compared with that at hover condition (Fig. 13), the distribution profile is symmetric and nearly the same as both distances.

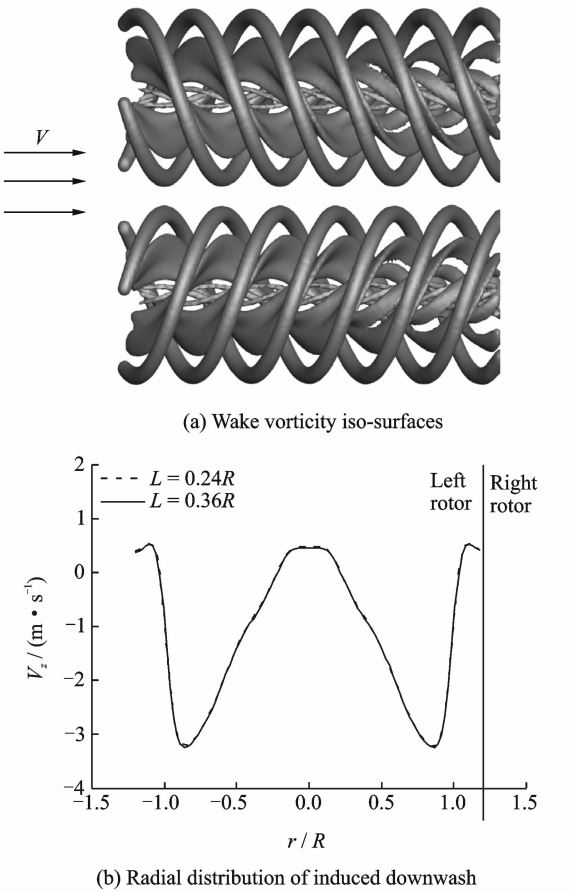

Fig. 14 Calculated results of airplane mode

3 CONCLUSIONS

In this paper, a new viscous vortex method is developed for tilt-rotor wake prediction in hover and airplane modes. The method is applied to several cases for both single rotor and dual-rotor calculations. From the calculated results presented in this study, the following conclusions can be drawn:

(1) The developed model can capture the fundamental characteristics of the rotor wake vorticity interaction, and is appropriate in simulating rotor with high twist blade such as tilt-rotor. Additionally, the predicted downwash also correlates well with the measurements.

(2) Because of the highly twisted blade design of tilt-rotor, the spanwise bound circulation distribution of the tilt-rotor is more smooth than that of the untwisted blade. Additionally, tip vortex strength of tilt-rotor is weaker than that of

traditional helicopter rotor due to the same reason.

(3) At hover condition, dual-tilt-rotor mutual interference will cause the appeareance of upward flow between the two rotors. This is an important formation reason of the tilt-rotor fountain flow effects.

(4) Dual-rotor mutual interference of tilt-rotor will break the tip vortex more earlier and lead it into unstable state. This may cause an unstable lift of tilt-rotor, and influence the flying qualities of the aircraft or even endanger the flight security.

(5) In airplane mode, the mutual interference of dual-rotor is very weak and its influence on rotor aerodynamic characteristics is almost negligible. Therefore single rotor case can be used in the theoretical analysis of tilt-rotor aerodynamic characteristics for the airplane mode.

References:

[1] Fejtek I, Roberts L. A CFD study of tilt rotor flowfields[R]. NASA-CR-186116, 1989.

[2] Strawn R C, Barth T J. A finite-volume Euler solver for computing rotary-wing aerodynamics on unstructured meshes[J]. Journal of the American Helicopter Society, 1993,38(2):61-67.

[3] Potsdam M A, Strawn R C. CFD simulations of tiltrotor configurations in hover[J]. Journal of the American Helicopter Society, 2005,50(1):82-94.

[4] Sheng C, Narramore J C. Computational simulation and analysis of bell Boeing quad tiltrotor aero interaction[J]. Journal of the American Helicopter Society, 2009,54(4):042002-042015.

[5] Narducci R, Jiang F, Liu J, et al. CFD modeling of tiltrotor shipboard aerodynamics with rotor wake interactions[R]. AIAA 2009-3857, 2009.

[6] Acree J R C. JVX proprotor performance calculations and comparisons with hover and airplane-mode test data[R]. NASA/TM-2009-215380, 2009.

[7] He C J, Zhao J G. Modeling rotor wake dynamics with viscous vortex particle method[J]. AIAA Journal, 2009,47(4):902-915.

[8] Zhao J, He C. A viscous vortex particle model for rotor wake and interference analysis[J]. Journal of the American Helicopter Society, 2010,55(1):1-14.

[9] Cottet G, Koumoutsakos P. Vortex methods: Theory and practice[M]. Cambridge: Cambridge University Press , 2000:55-89.

[10] Mas-Gallic S. Contribution à l'analyse numérique des méthodes particulaires[D]. La Canada: Université Pierre-et-Marie-Curie, 1987. (in French)

[11] Lindsay K T. A three-dimensional cartesian tree-code and applications to vortex sheet roll-up[D]. Michigan: University of Michigan, 1997.

[12] Greengard L, Rokhlin V. A fast algorithm for particle simulations[J]. Journal of Computational Physics, 1987,73(2):325-348.

[13] Felker F F, Signor D B, Young L A, et al. Performance and loads data from a hover test of a 0.658-scale V-22 rotorand wing[R]. NASA TM 89419, 1987.